THE UNIVERSITY OF RHODE ISLAND

Mechanical, Industrial & Systems Engineering

Technology Showcase

Microfluidics and microsystems for environmental monitoring and human health

Yang Lin, Ph.D. /Assistant Professor
College of Engineering
University of Rhode Island

04/18/2023

THINK BIG WE DO™

Who am I?

Yang Lin

Assistant Professor, URI
(2020 to Present)

Postdoctoral research associate at UIC
(January 2020 – August 2020)

Ph.D. (2019) in Mechanical Engineering
University of Illinois at Chicago (UIC)

M.S. (2015) in Mechatronic Engineering
B.S. (2012) in Mechanical Engineering
China

Research Interests

Microfluidics and Lab-on-a-Chip

Acoustofluidics

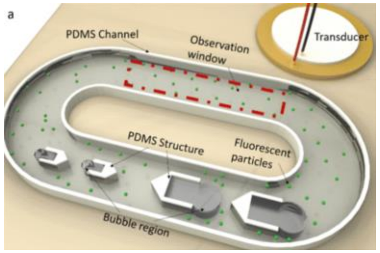

Biosensors

Environmental monitoring

Point-of-care

Microfabrication

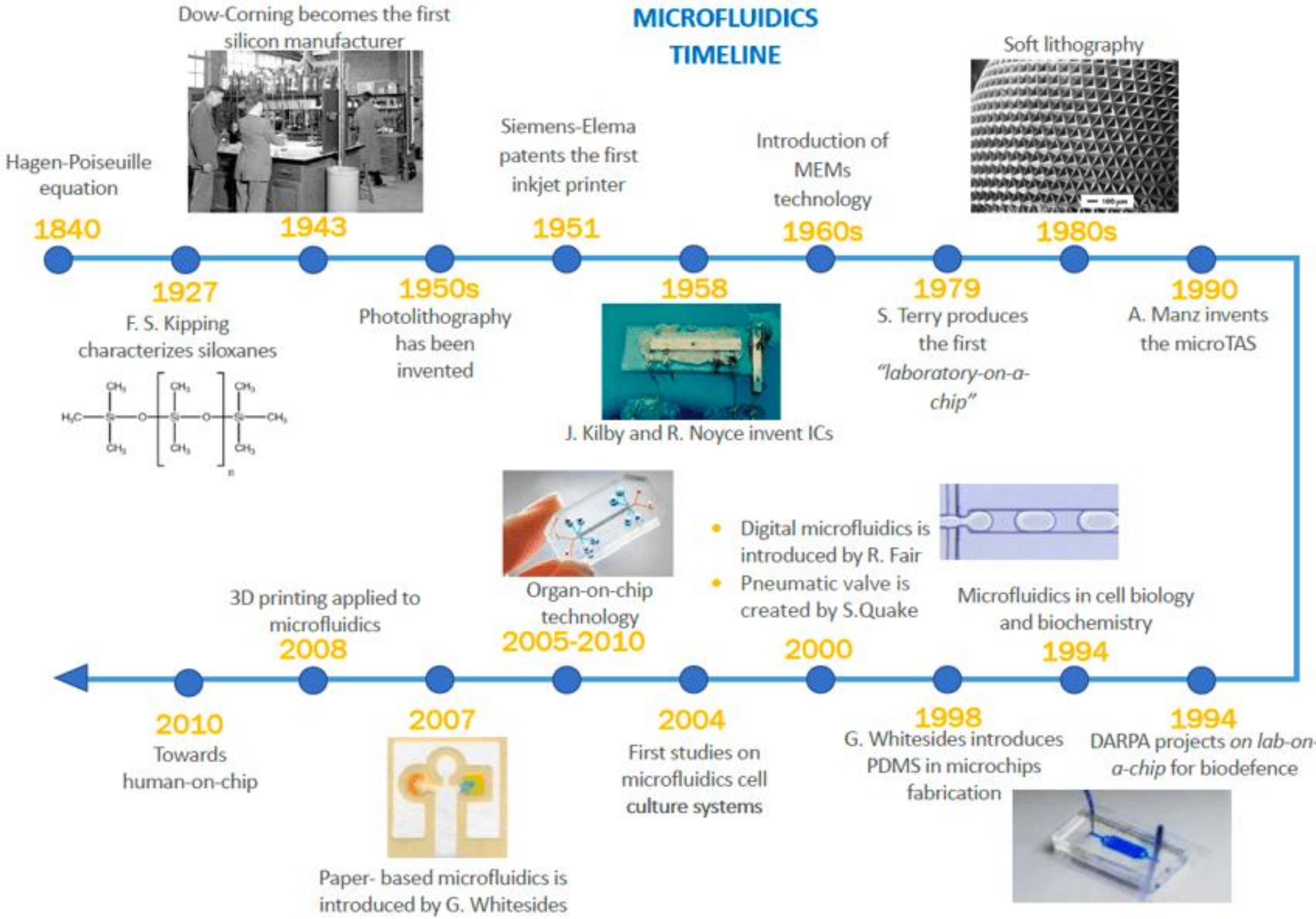
MICROFLUIDICS
TIMELINE
1840
Hagen-Poiseuille equation
1927
F. S. Kipping characterizes siloxanes
1943
Dow-Corning becomes the first silicon manufacturer
1950s
Photolithography has been invented
1951
Siemens-Elema patents the first inkjet printer
1958
J. Kilby and R. Noyce invent ICs
1960s
Introduction of MEMs technology
1979
S. Terry produces the first "laboratory-on-a-chip"
1980s
Soft lithography
1990
A. Manz invents the microTAS
1994
DARPA projects on lab-on-a-chip for biodefence
1994
Microfluidics in cell biology and biochemistry
1998
G. Whitesides introduces PDMS in microchips fabrication
2000
Digital microfluidics is introduced by R. Fair
Pneumatic valve is created by S.Quake
2004
First studies on microfluidics cell culture systems
2005-2010
Organ-on-chip technology
2007
Paper- based microfluidics is introduced by G. Whitesides
2008
3D printing applied to microfluidics
2010
Towards human-on-chip

Advantages of Microfluidics

- Low sample and reagent consumption; fluid volumes (μl; nl; pl; fl)
- Fast analysis, efficient detection
- Portable and compact devices

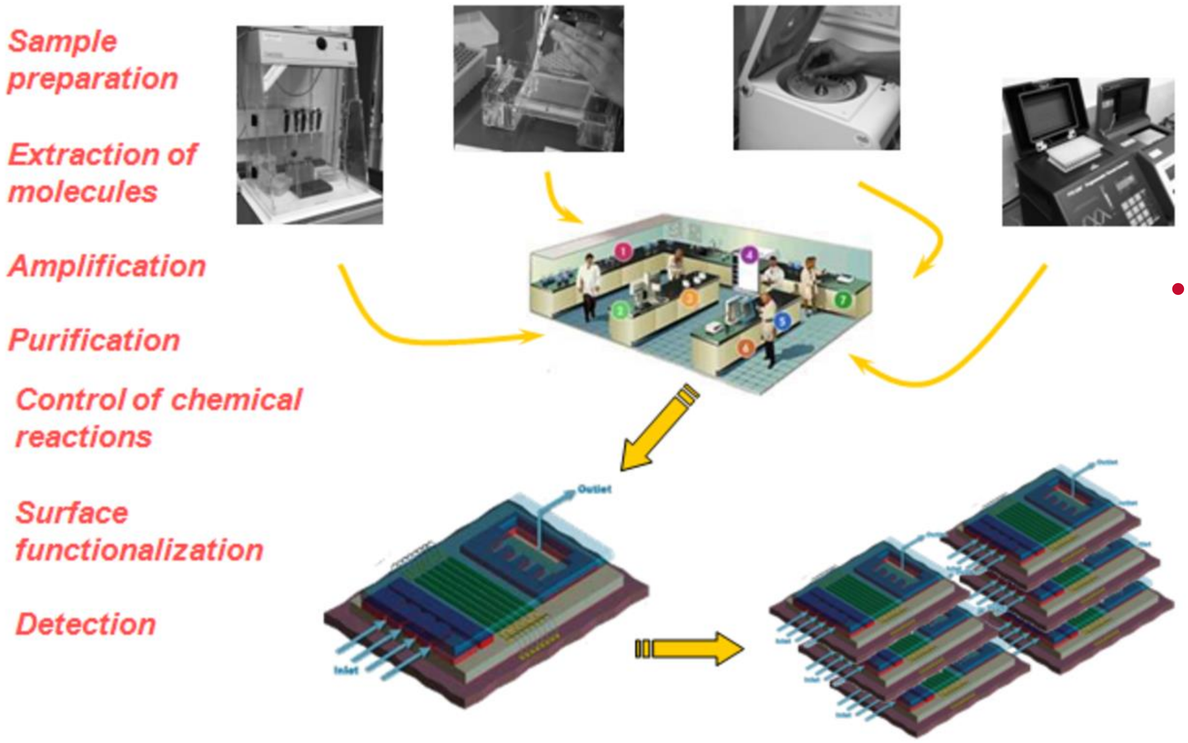

- Integration of various functional units – making a "**Lab on a Chip**" device

Acoustic particle and flow manipulation

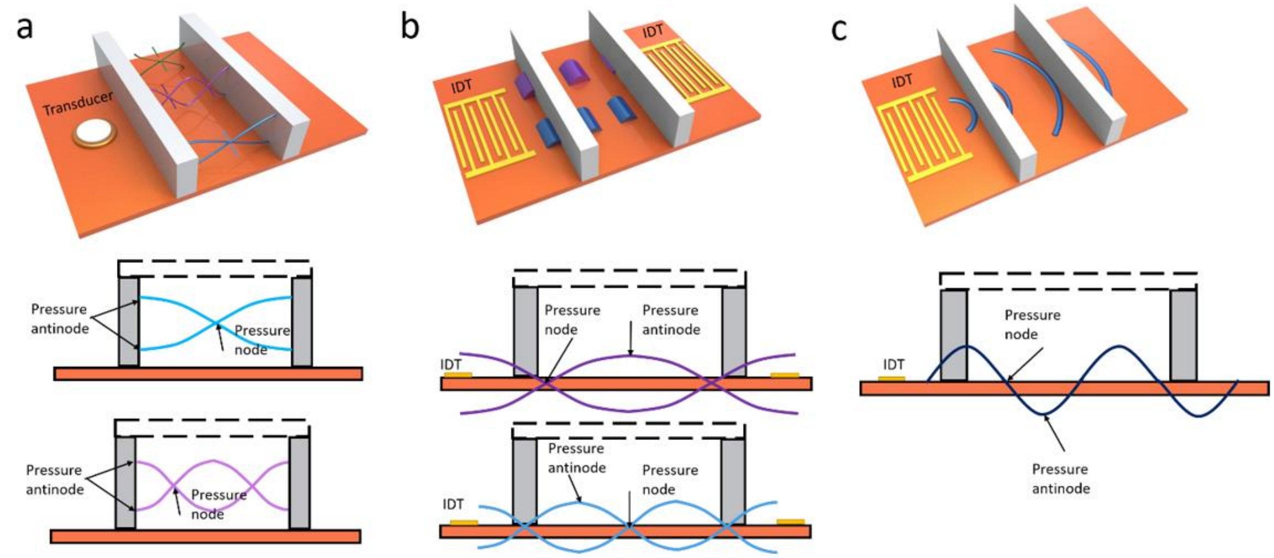

Bulk acoustic waves | *Standing SAW* | *Travelling SAW*

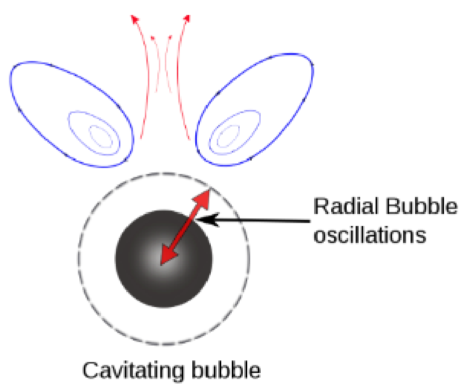

Acoustic secondary radiation force

$$F_{SRF} = 4\pi\rho_l \frac{\rho_l - \rho_p}{\rho_l + 2\rho_p} \frac{{R_b}^4 R_p^3}{d^5} \omega^2 \xi^2$$

Micromixer on flexible foil

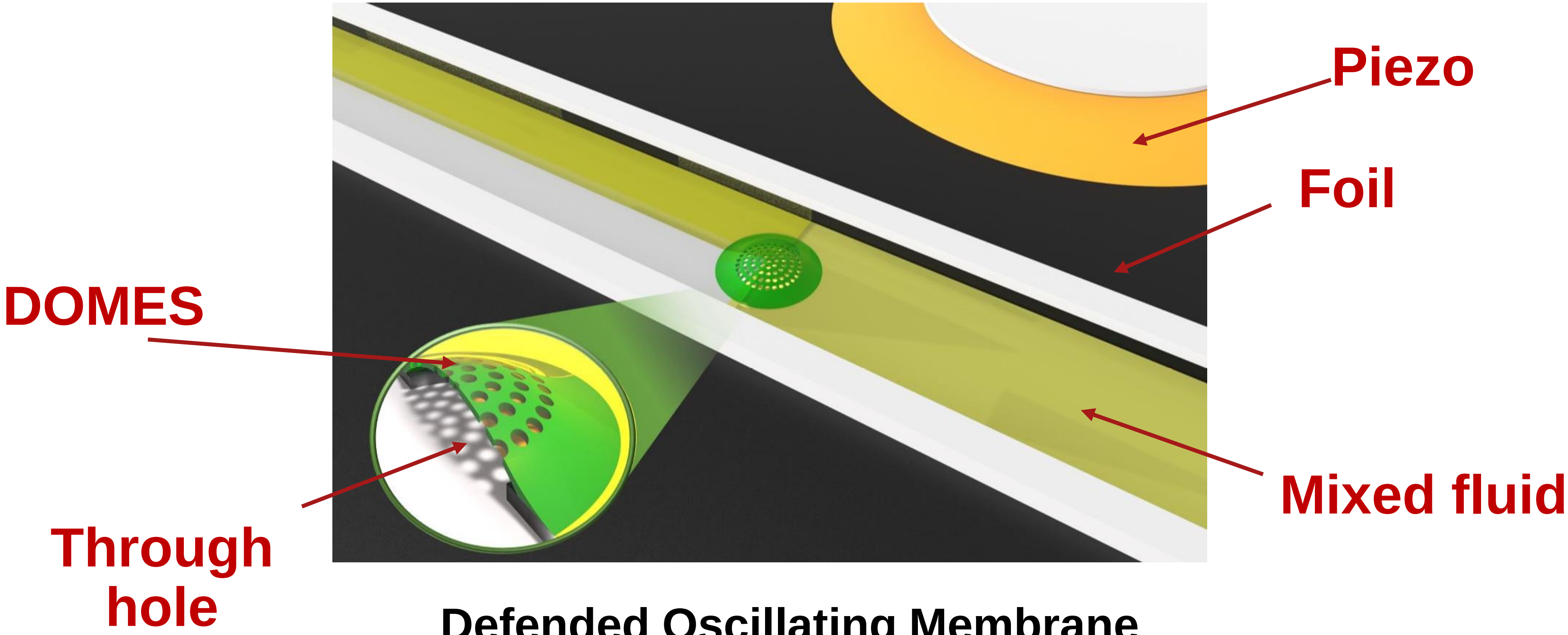

Defended Oscillating Membrane Equipped Structures (DOMES)

Mixing performance

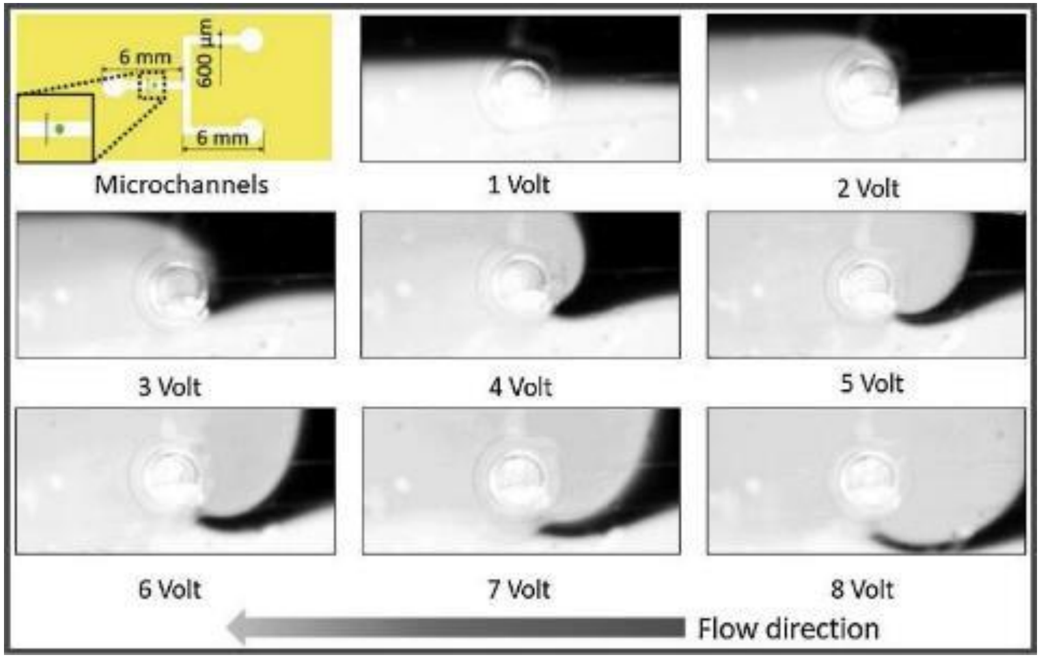

- The intensity of the microstreaming grew with the driving voltage.
- Mixing performance increased along with increase of driving voltage.

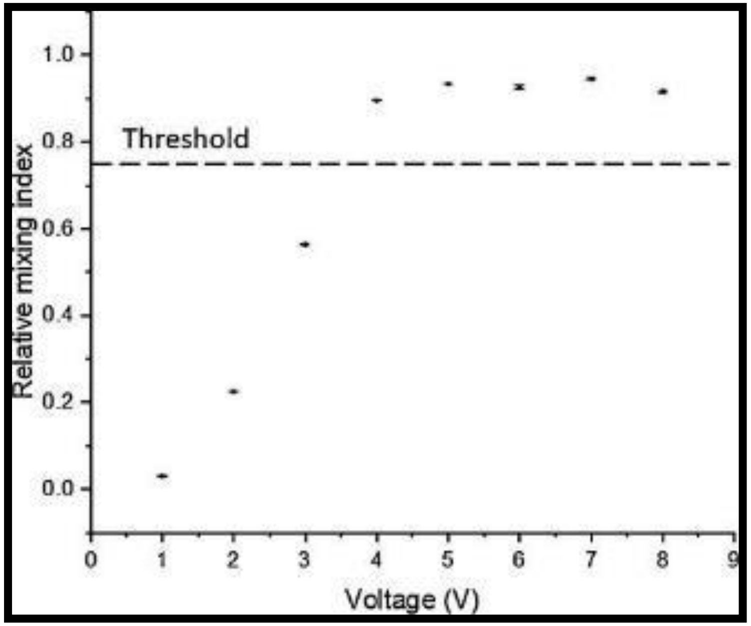

- Relative mixing index (RMI) was calculated at a measuring line after mixing.

$$RMI = 1 - \frac{\sqrt{\frac{1}{N}\sum_{i=1}^{N}(I_i - \langle I \rangle)^2}}{\sqrt{\frac{1}{N}\sum_{i=1}^{N}(I_{oi} - \langle I_o \rangle)^2}}$$

- RMI increased with increase of driving voltage.

Bidirectional micropump

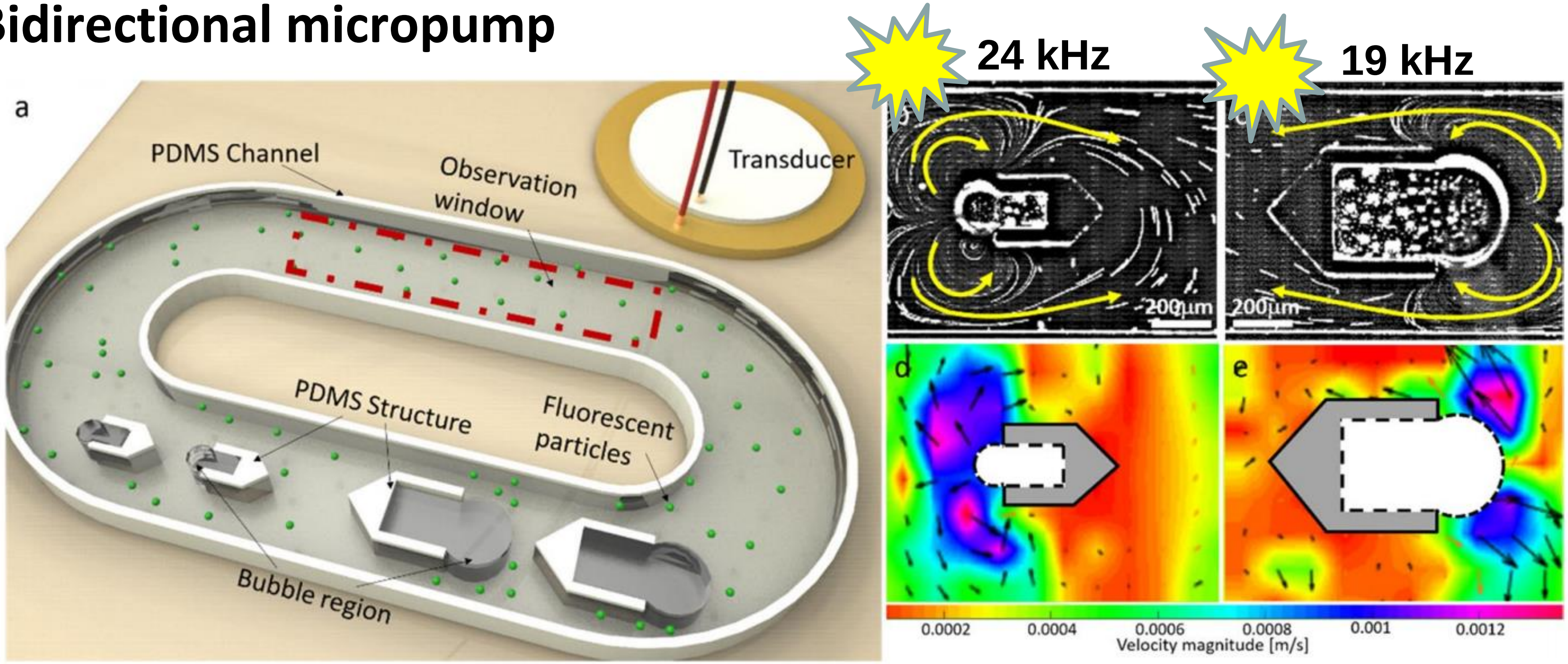

The strongest microstreaming can be produced when the excited frequency is close to the resonant frequency of the bubble, which of a bubble can be estimated by Minnaert eigenfrequency equation: (Minnaert 1933)

$$f_0 = \frac{1}{2\pi a}\sqrt{\frac{3\gamma P_0}{\rho}}$$

f_0: resonant frequency

a: radius of the bubble

γ: polytropic exponent, 1.4 for air bubble

P_0: ambient pressure

ρ: density of the liquid

a ↓ **Resonant frequency** ↑

The microplastics cycle

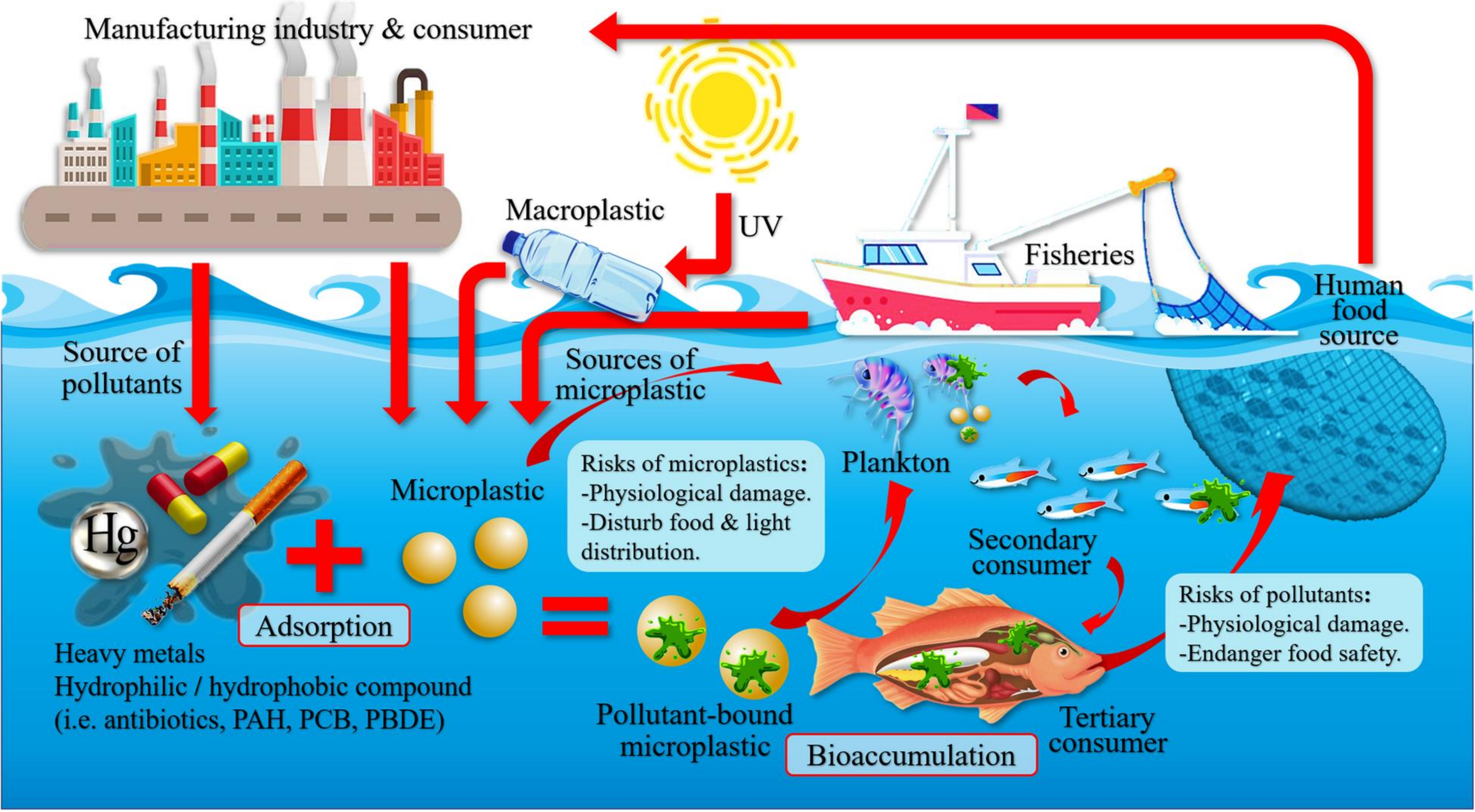

Amelia, T.S.M. *et. al.* Marine Microplastics as Vectors of Major Ocean Pollutants and Its Hazards to the Marine Ecosystem and Humans. *Prog. Earth Planet. Sci.* **2021**.

Microplastics in human blood

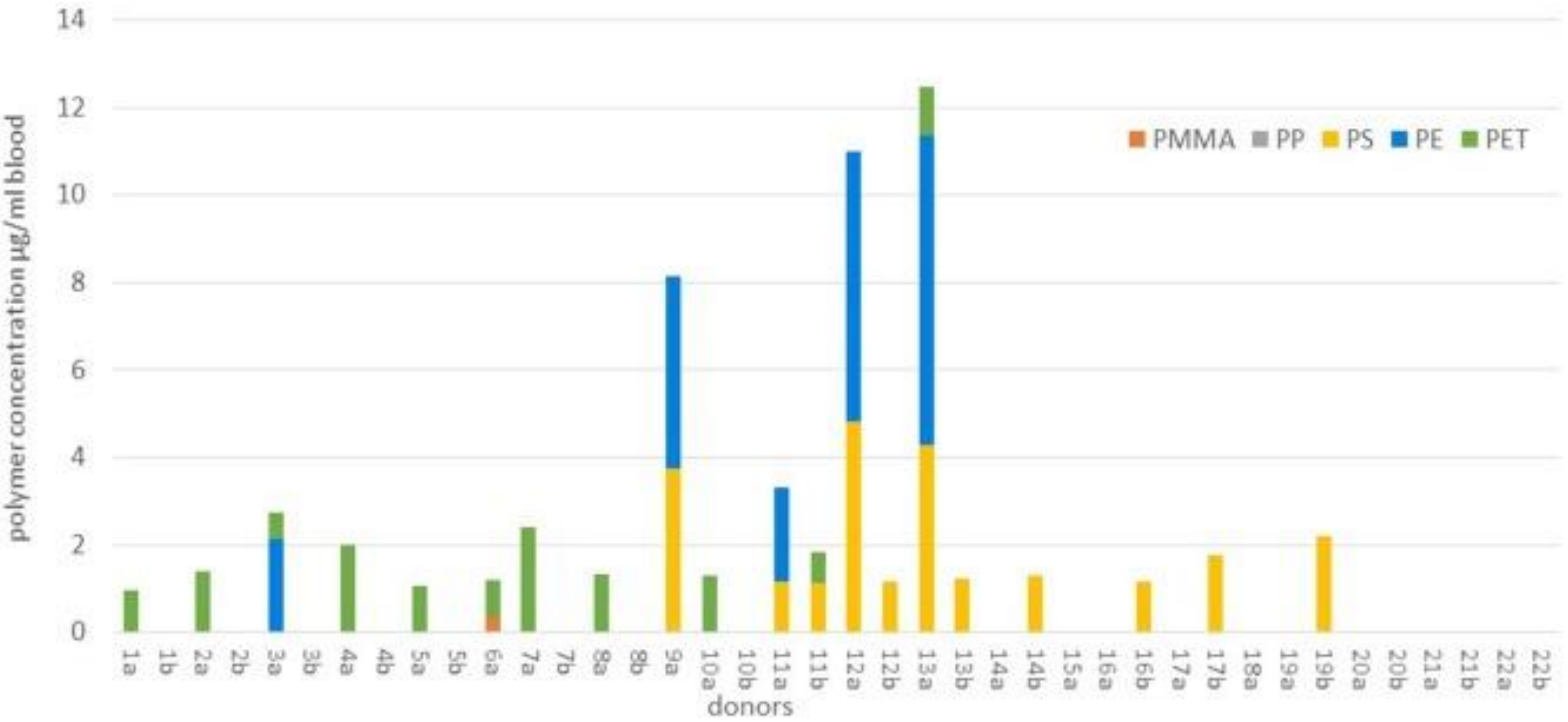

Leslie, Heather A., *et al*. "Discovery and quantification of plastic particle pollution in human blood." *Environment international* **2022**.

Acoustofluidic separation for microplastics

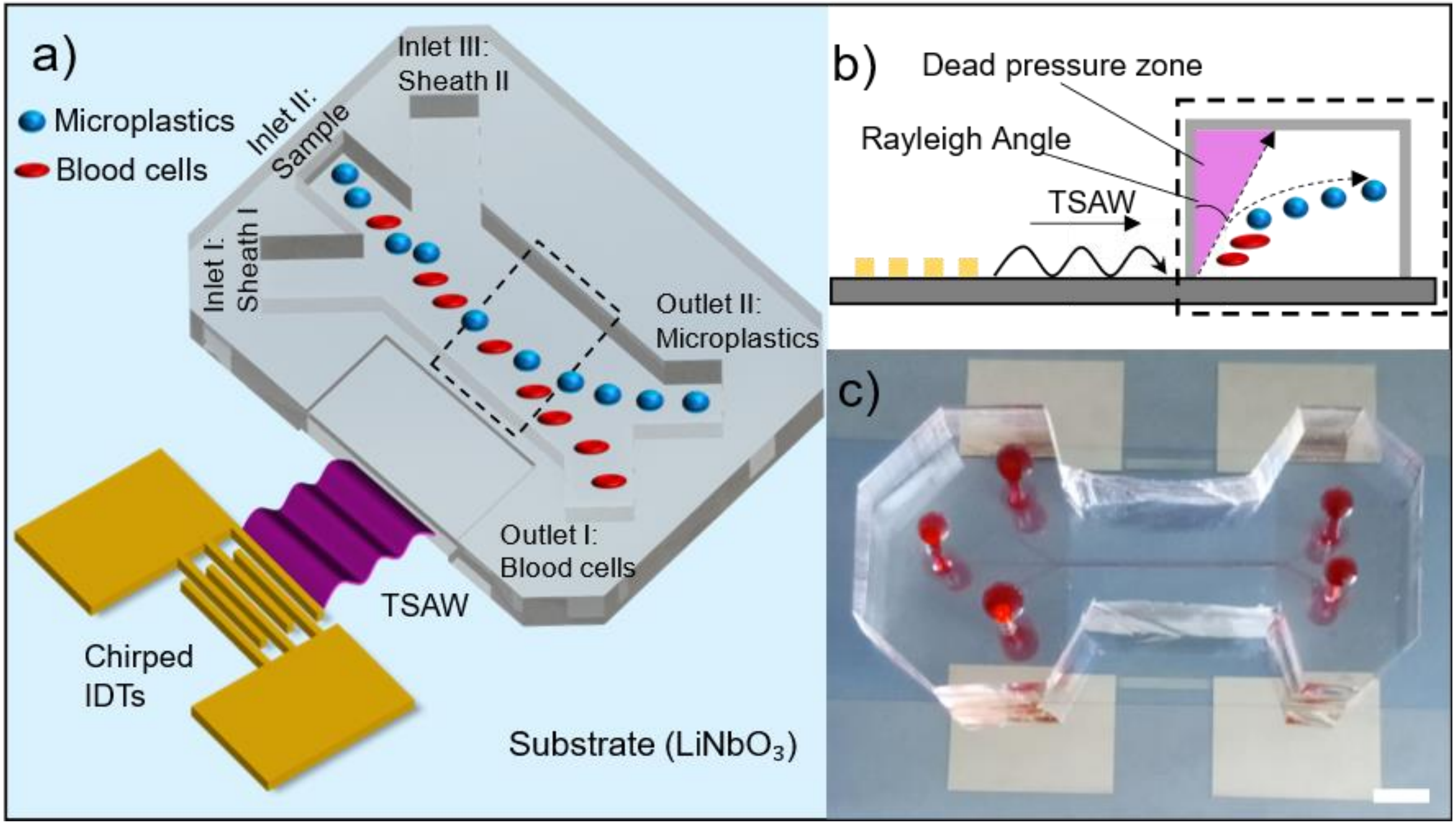

The microfluidic device used for blood microplastics separation. a) Schematic of the separation mechanism. Once the IDTs are actuated by electrical signals, the TSAW is established on the substrate surface and will displace the particles according to their physical properties (i.e., size, compressibility, *etc.*). The separation is achieved if the microplastics particles have higher ARF than blood cells with the same operational frequency (larger displacements of microplastic particles). b) Cross-sectional view of the separation process. The TSAW causes a pressure gradient that displaces the microplastics towards the separation region. Due to the Rayleigh angle, there is a dead pressure zone that traps particles and hinders their separation. This region is avoided with the use of Sheath flow I. c) Photo of the actual device. Scale bar is 5 mm.

Mathematical Modelling

$$F_{TSAW} = Y_P \pi a^2 \bar{E} \qquad (1)$$

$$Y_P = \frac{4}{{x_0}^2} \sum_{n=0}^{\infty} \{(n+1)(V_n^{'} U_{n+1}^{'} - U_n^{'} V_{n+1}^{'}) {x_0}^2 - n(n+1)(n+2)(V_n U_{n+1} - U_n V_{n+1}) + [n(n+1)(U_n V_{n+1}^{'} - V_n U_{n+1}^{'}) - (n+1)(n+2)(U_n^{'} V_{n+1} - V_n^{'} U_{n+1})] x_0 + (n+1)(V_n U_{n+1} - U_n V_{n+1}) {x_0}^2\} \qquad (2)$$

$$x_{0,1,2} = \frac{2\pi f a}{c_{f,l,s}} \qquad (3)$$

Y_P = Acoustic Radiation Factor

a = Particle Radius

E = Mean Acoustic Energy

V = Bessel function (1st kind)

U = Bessel function (2nd kind)

x = Helmholtz number

f = Frequency

c = speed of sound

Theoretical Calculation of the Acoustic Radiation Factor

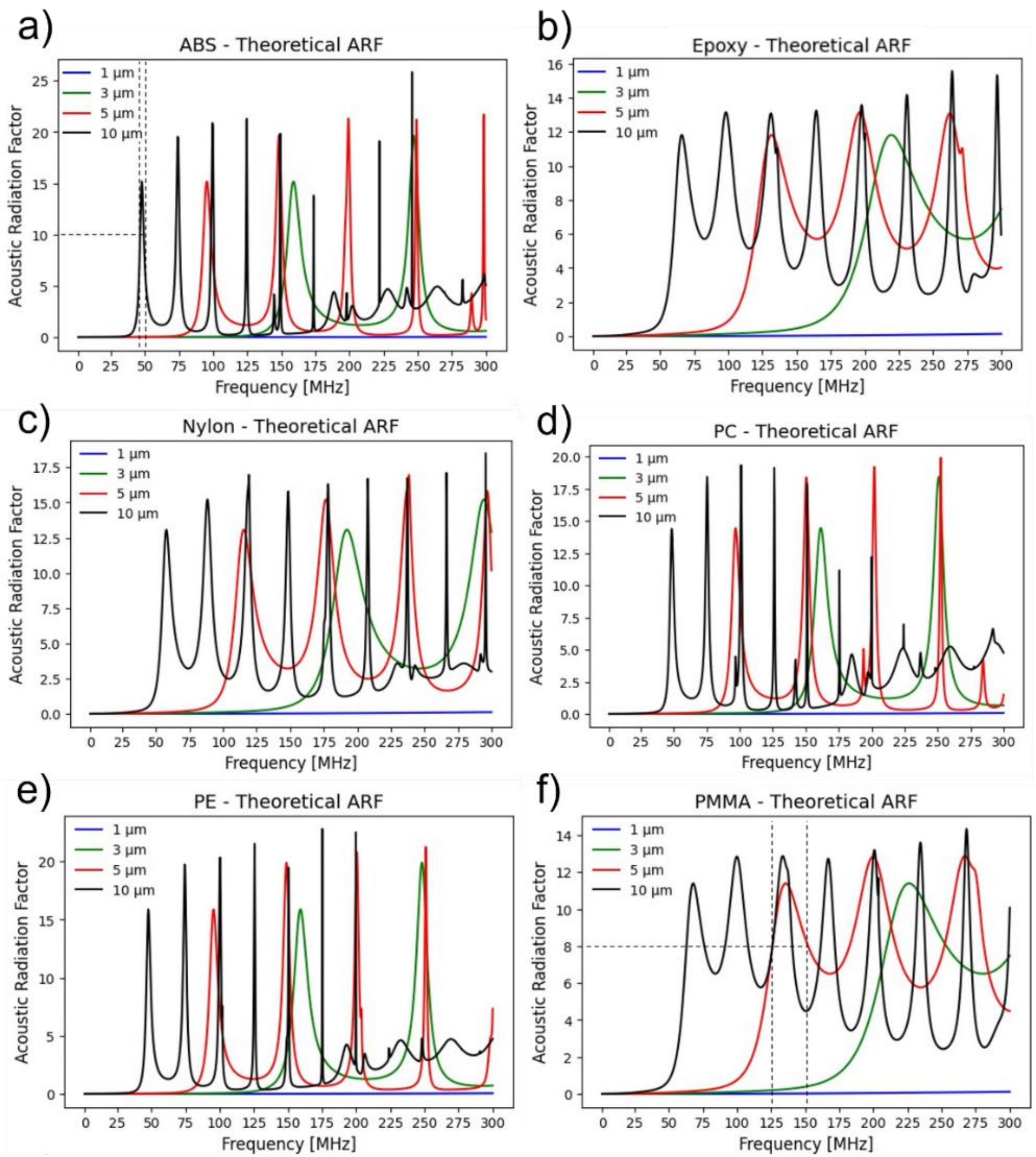

The theoretical ARFs of microplastics of different types and sizes as a function of the input frequency. The results suggested that the minimum frequency required to produce significant ARF increases as the particle size decreases for all types of microplastics studied here. a) ABS. b) Epoxy. c) Nylon. d) PC. e) PE. f) PMMA. g) PP. h) PVC. i) PS. j) Teflon.

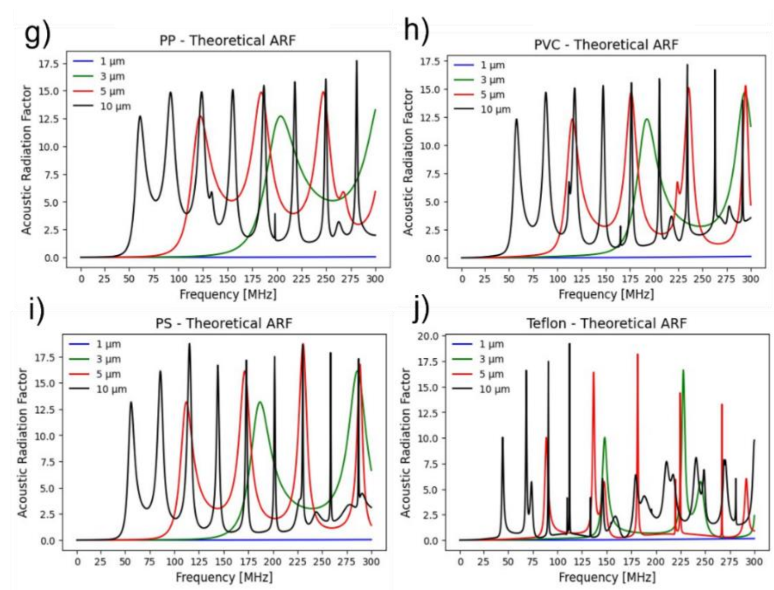

Experimental Validation of the Acoustic Radiation Factor

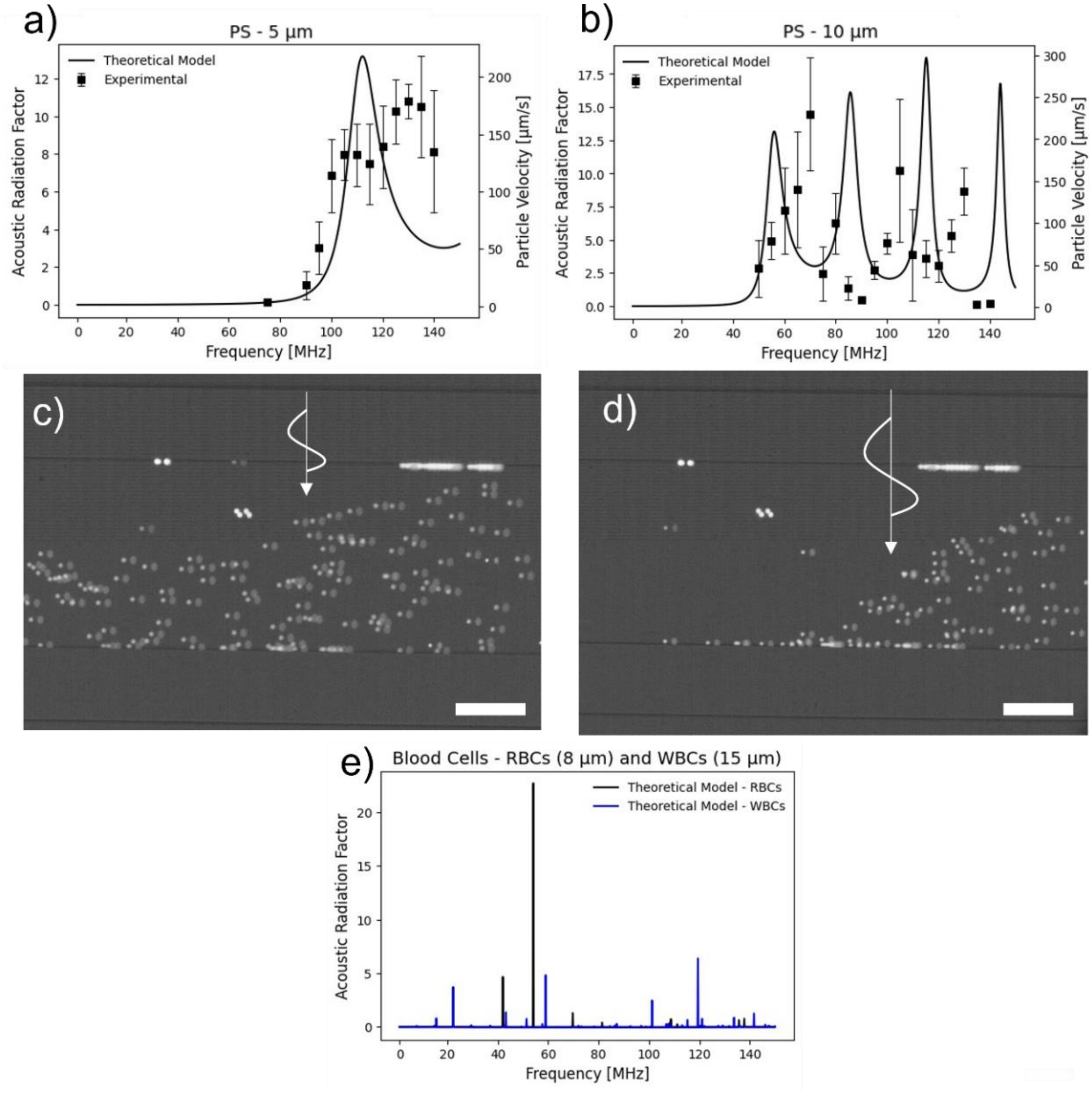

Comparison between the theoretical prediction of ARF and experimental particle velocity. a) Comparison between theoretical ARF and particle velocity for 5 µm polystyrene particles. b) Comparison between theoretical ARF and particle velocity for 10 µm PS particles. c) Displacement of 5 µm PS particles at 95 MHz. The scale bar is 100 µm. d) Displacement of 5 µm PS particles at 125 MHz. The higher ARF values at 125 MHz induce higher displacements in the particles than 95 MHz. The white arrow indicates the direction of the TSAW. The scale bar is 100 µm. e) Theoretical ARF for red and white blood cells. Blood cells were experimentally tested at resonant frequencies of microplastics such as 125 MHz, no significant displacement was observed.

Blood Microplastics Separation using TSAW – Experimental Results

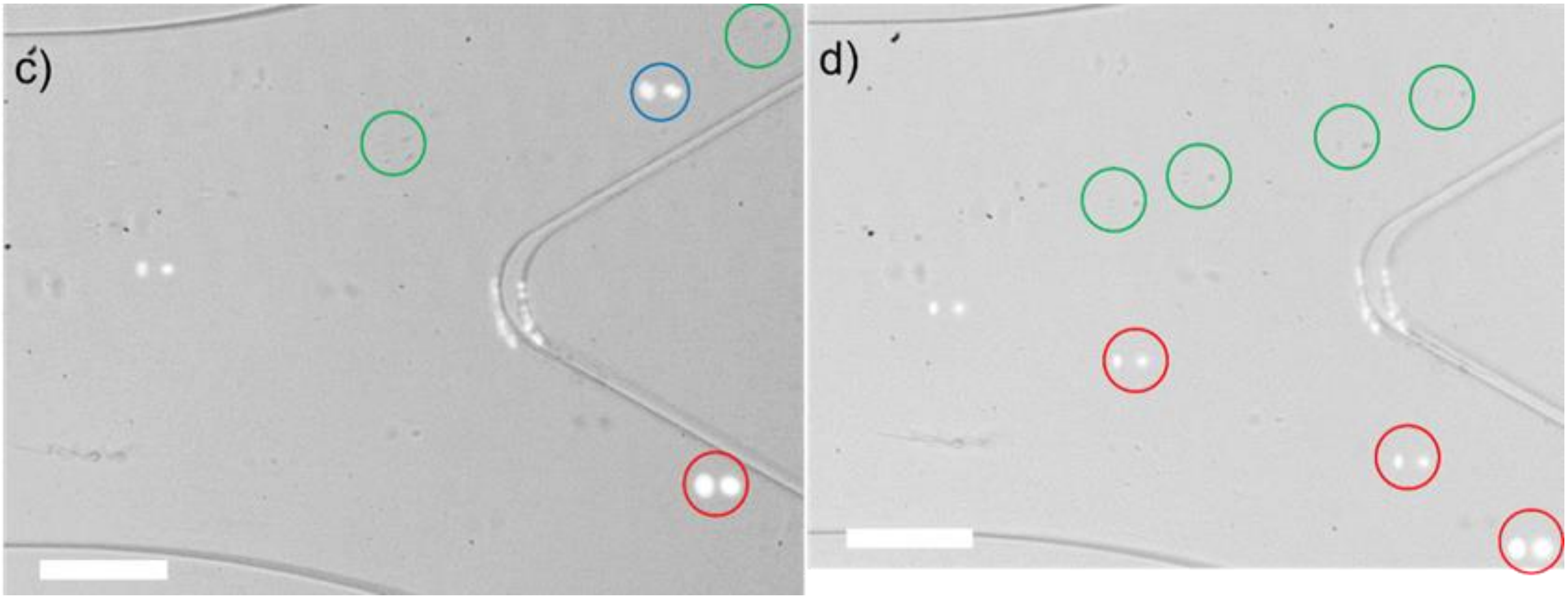

Blood PS separation using 128 MHz, 50% power, and 10 µL/min. Using this operation setup, the separation could not overcome performances of 60%. The image shows a 5 µm PS particle (circled in blue) being deflected towards the wrong outlet, while the 10 µm particle (circled in red) was deflected towards the correct microplastics outlet. The particles circled in green were blood cells. Scale bar is 100 µm. d) Blood PS separation using 128 MHz, 50% power, and 1 µL/min. Reducing the flow rate considerably increased the separation efficiency, achieving values close to 100%. The image shows that both 5 and 10 µm PS particles (circled in red) were displaced towards the microplastic collection outlet. The particles circled in green were blood cells. Supplementary Information contains videos demonstrating the separation process. Scale bar is 100 µm.

Static and Microfluidic staining

Schematic illustration of the staining processes

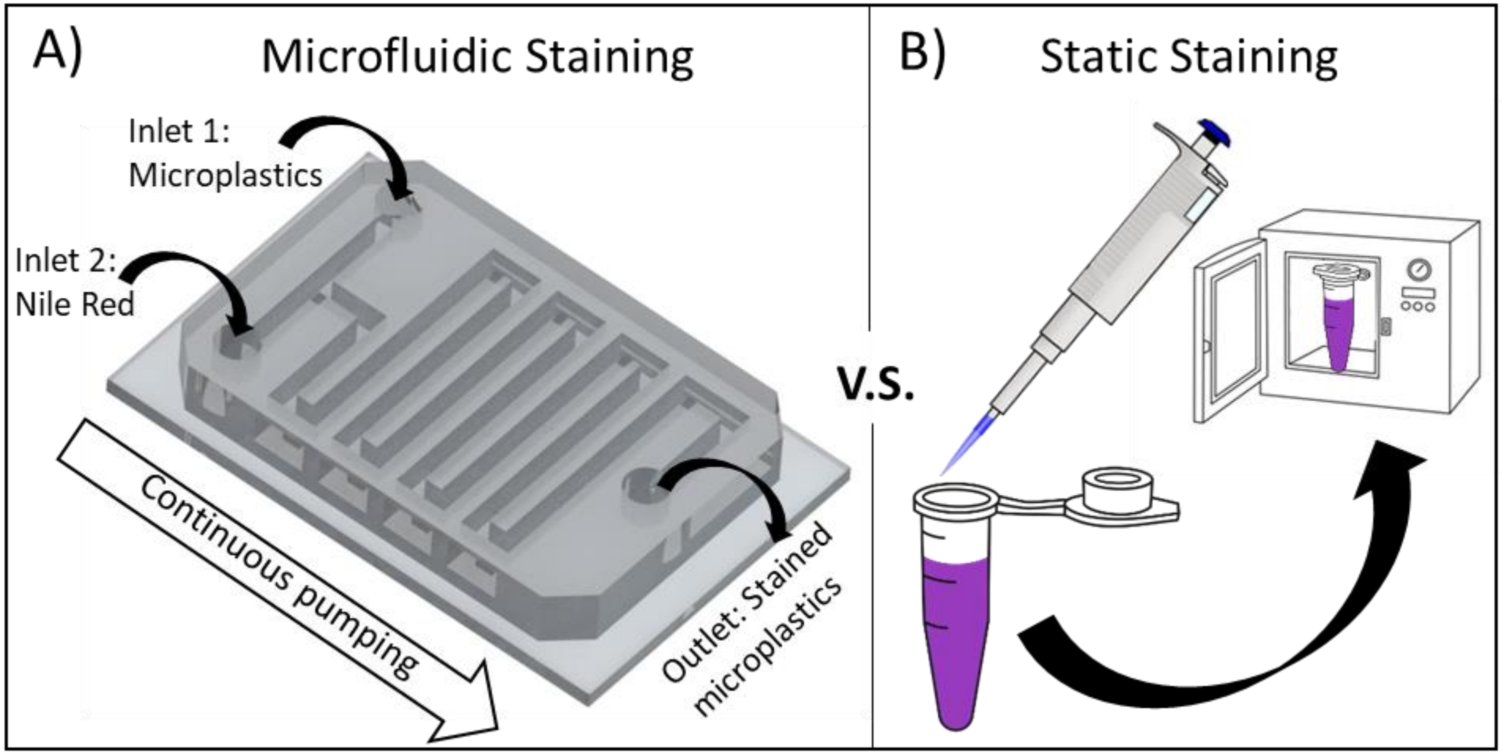

A) Process of microfluidics-based continuous staining of microplastics using Nile Red.

B) Process of static staining of microplastics.

Compared to microfluidic staining, the static process is laborious as it requires multiple batches and manual operation.

Continuous identification: Microfluidic staining

Microfluidic staining for different plastics and yeast

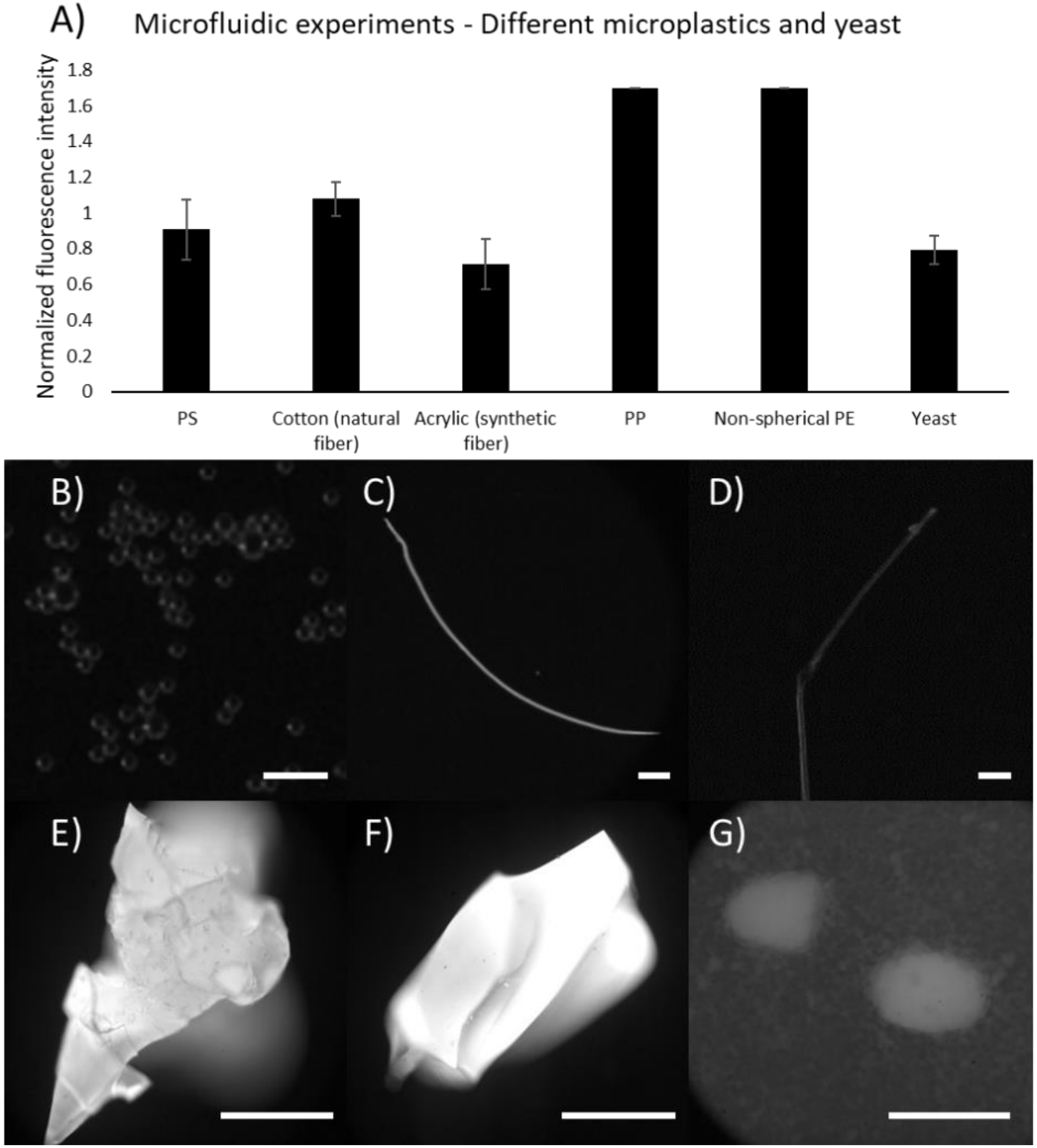

A) Fluorescence levels for different microplastics and yeast;

B) PS microspheres; Scale bar is 50 μm;

C) Cotton (natural fiber);

D) Acrylic (synthetic fiber); Scale bars are 1 mm;

E) PP from storage container; Scale bars are 50 μm.

F) PE from storage container; Scale bars are 50 μm.

G) Yeast; Scale bars are 50 μm.

Microfluidic Hydrodynamic Particle Trapping Device

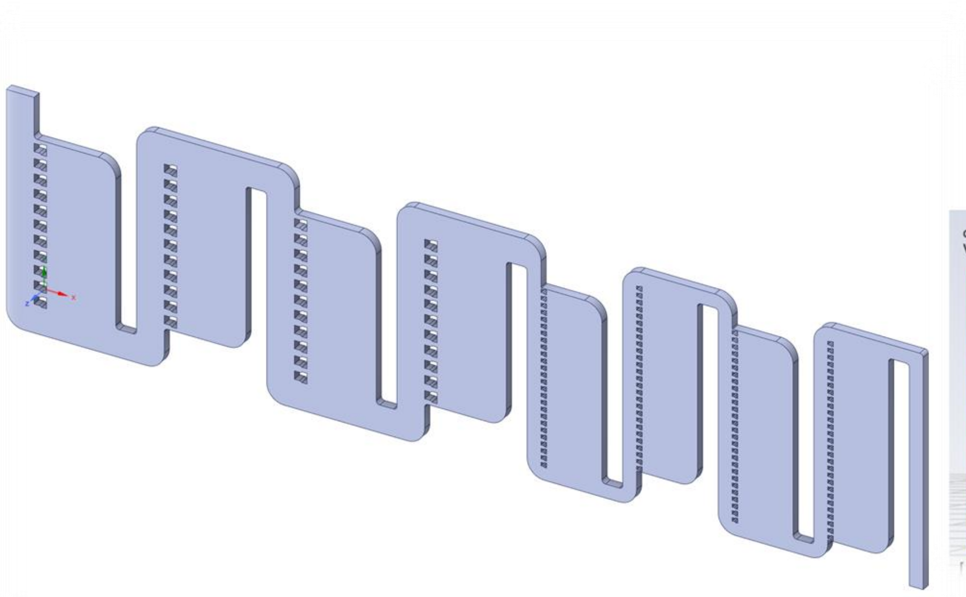

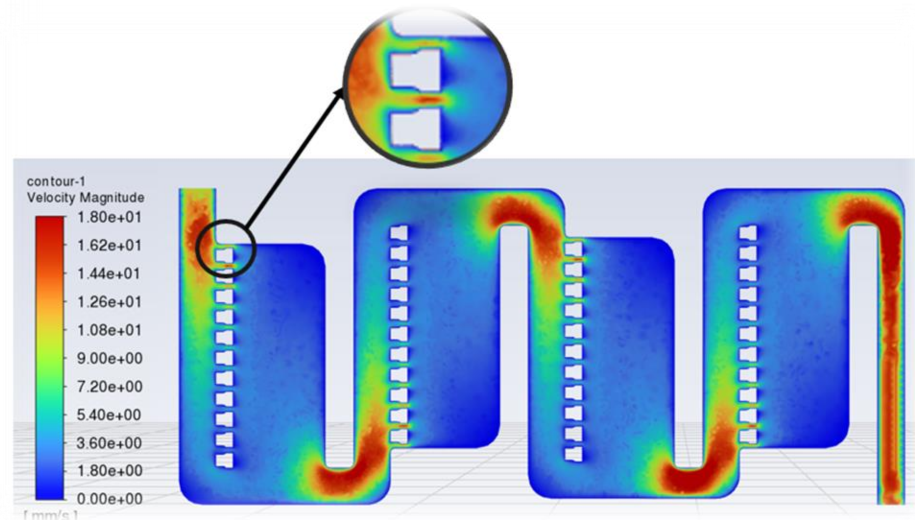

Fluid velocity distribution

Fabrication:

- Standard soft lithography
- PDMS channel

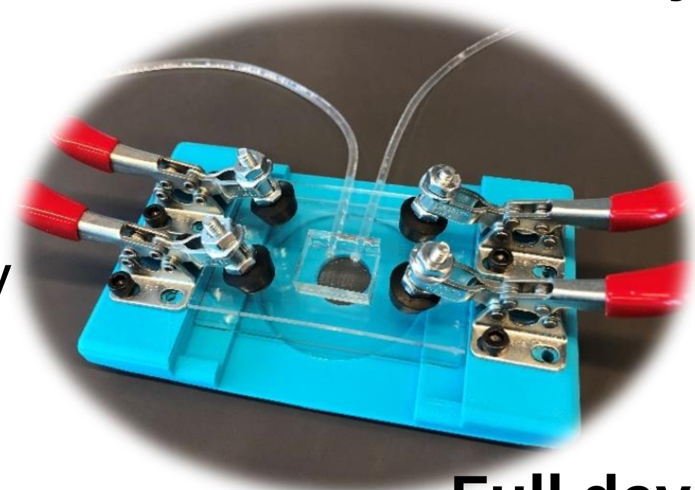

Full device assembly

Chemical characterization

Confocal Raman Spectroscopy

Chemical analytical technique used for material characterization.

Advantages:

- Capable of identifying particles smaller than 1µm.
- Compatibility with liquid sample

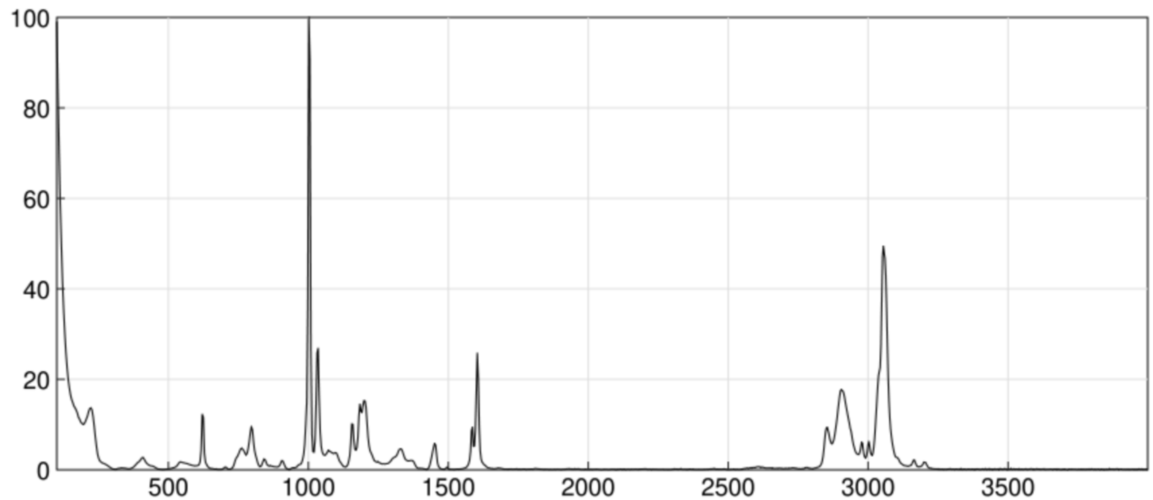

Raman Spectrum of Pristine Polystyrene

Support Vector Machine (SVM)	Random Forest (RF)	Convolutional Neural Network (CNN)	Residual Neural Network (ResNet)
• Easy to train • Good accuracy	• Work with large datasets	• High accuracy	• High Robustness

Original Train Dataset				
Material Type	pristine	SLOPP	Mendeley	Total
Polystyrene (PS)	30	11	1	42
Polypropylene (PP)	30	17	51	98
polyethylene terephthalate (PET)	30	9	0	39
polyester (PEST)	30	10	16	56
polyamide (PA, nylon)	30	7	4	41
polycarbonate (PC)	30	7	2	39
polyethylene (PE)	30	24	68	122
polyurethane (PU)	30	6	0	36
polyvinyl chloride (PVC)	30	11	8	49
poly(methyl methacrylate)(PMMA)	30	1	0	31
cellulose acetate (CA)	30	4	0	34

- **Identification of mixed pristine PE & PS microspheres**

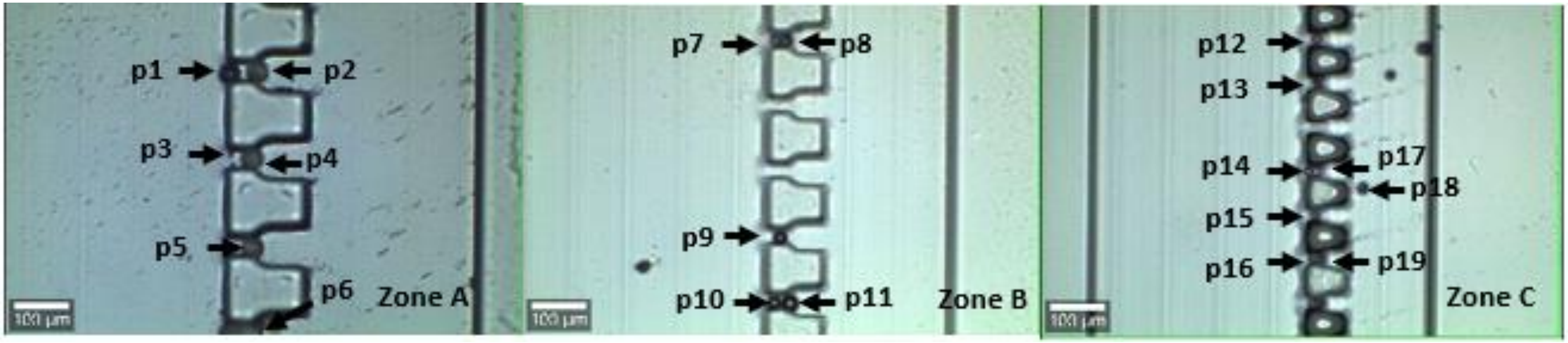

	SVM	CNN
P1	PE	100.00%PE
P2	PE	100.00%PE
P3	PS	100.00%PS
P4	PE	100.00%PE
P5	PE	100.00%PE
P6	PE	100.00%PE

	SVM	CNN
P7	PE	100.00%PE
P8	PE	100.00%PE
P9	PE	100.00%PE
P10	PE	100.00%PE
P11	PE	100.00%PE

	SVM	CNN
P12	PE	100.00%PE
P13	PS	100.00%PS
P14	PE	100.00%PE
P15	PS	100.00%PS
P16	PS	100.00%PS
P17	PE	100.00%PE
P18	PS	100.00%PS
P19	PE	100.00%PE

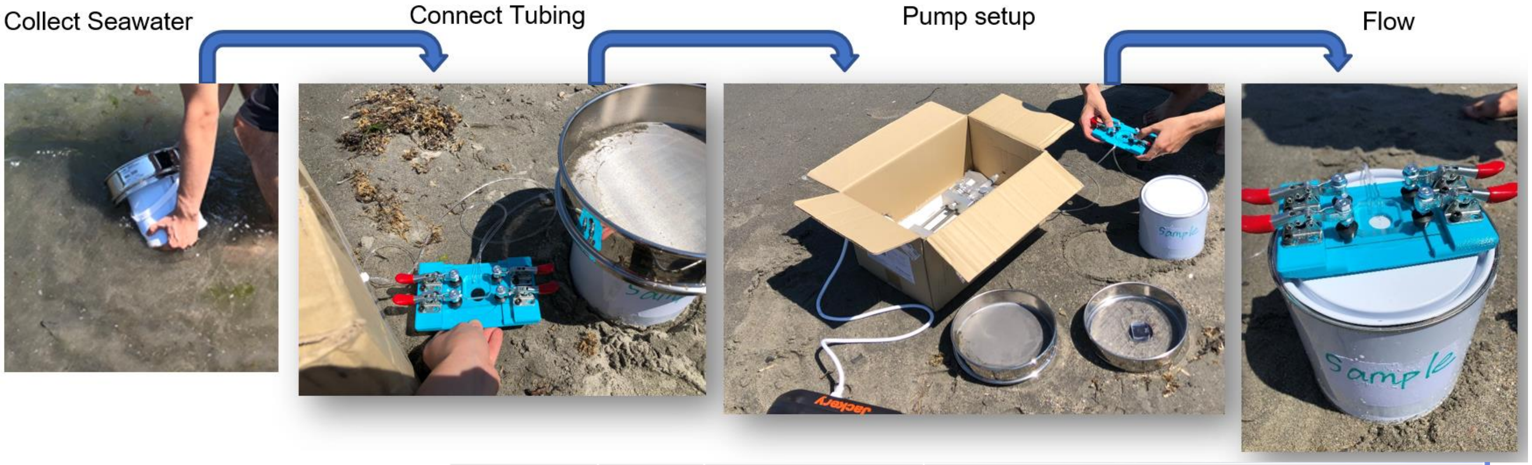

Identification Results

Particle	SVM	CNN	KnowItAll
P1	PE	100% PE	52.79% 2-(Ethylsulfonyl) ethanol; 52.55% p-(Ethylene); 51.25% Phosgenite
P2	PE	100% PE	63.37% Thallium(I) chloride; 63.24% Ammonium hexachloroplumbate; 57.22% MS 455;
P3	CA	100%CA	71.3% Zinc Oxide; 70.47% Cellulose, microcrystalline; 69.63% Cellulose;
P4	PE	72.42%PE 27.58% PS	62.56% Poly (ethylene-co-vinyl acetate),14 wt. % vinyl acetate; 61.14% p-(Acrylic acid); 60.01% MS 455
P5	CA	69.88% Polyester; 23.67% CA; 6.45% PP	71.96% Cellulose, microcrystalline; 67.52% Sodium borohydride on aluminum oxide; 66.73% Cellulose Acetate sorbate

- # Impact of microplastics on human health

Study	Cell line	Particles used	Tests performed	findings
Size-dependent neurotoxicity of micro- and nano-plastics in vitro microfluidic	Ht22	Commercial pristine PS mp (1um) and np 100nm) at various concentration 5, 25, 75 ug/ml	Apoptosis, ROS, viability, cell cycle Static and dynamic loading. Flow condition increases uptake efficiency	Mp no effect on viability, size effect linked with ROS and S phase arresting
Cytotoxicity and pro-inflammatory effect of PS nanopalstics and micro on RAW264.7	RAW264.7	Commercial pristine PS mp (3um) and np 80nm) 5, 10 ug/L	Apoptosis, viability, cytokines THF-α, IL-6, 10, NO synthesis, ROS.	NP effects > MPs; NP and MP showed different impacts on the induction of cytokine release;
Polystyrene microplastics induce immunometabolic active state in macrohage	C57BL	Comercial 10 um PS green fluorescence	FACS uptake, glycolytic rate, particle degradation in the cell, phagocytosis	Metabolic shift toward glycolysis, reduction of mitochondrial respiration, increase of cytokine gene expression

Most on PS

Our method

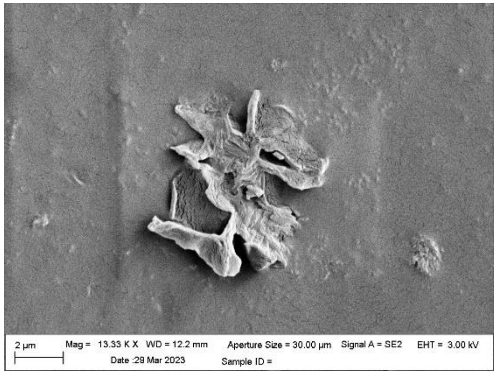
2 µm
Mag = 13.33 K X
WD = 12.2 mm
Aperture Size = 30.00 µm
Signal A = SE2
EHT = 3.00 kV
Date :29 Mar 2023
Sample ID =

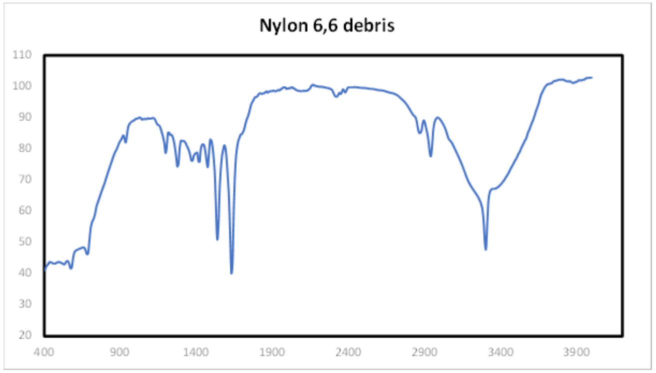
Nylon 6,6 debris
110
100
90
80
70
60
50
40
30
20
400
900
1400
1900
2400
2900
3400
3900

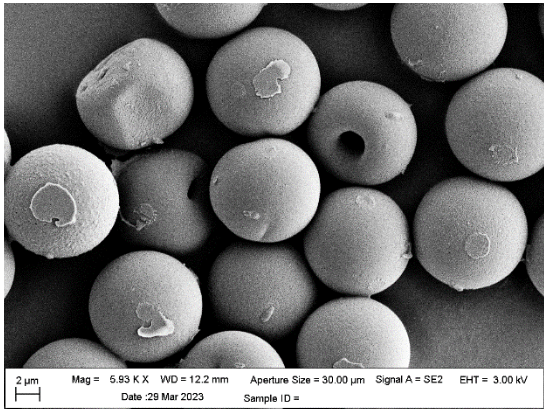
2 µm
Mag = 5.93 K X
WD = 12.2 mm
Aperture Size = 30.00 µm
Signal A = SE2
EHT = 3.00 kV
Date :29 Mar 2023
Sample ID =

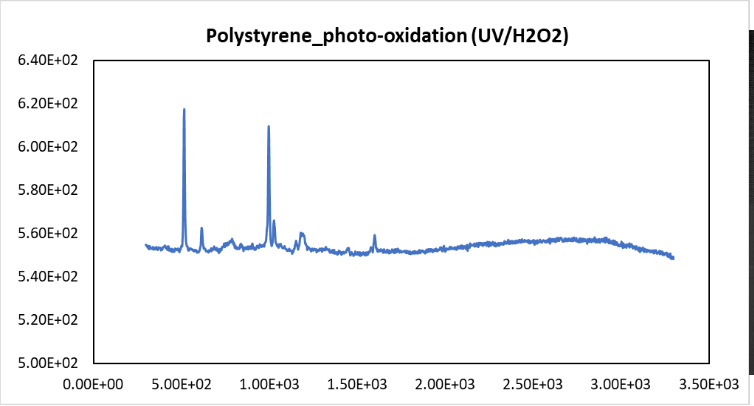
Polystyrene_photo-oxidation (UV/H2O2)
6.40E+02
6.20E+02
6.00E+02
5.80E+02
5.60E+02
5.40E+02
5.20E+02
5.00E+02
0.00E+00
5.00E+02
1.00E+03
1.50E+03
2.00E+03
2.50E+03
3.00E+03
3.50E+03

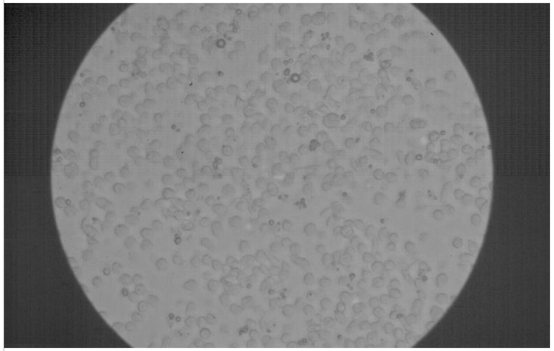

Our method

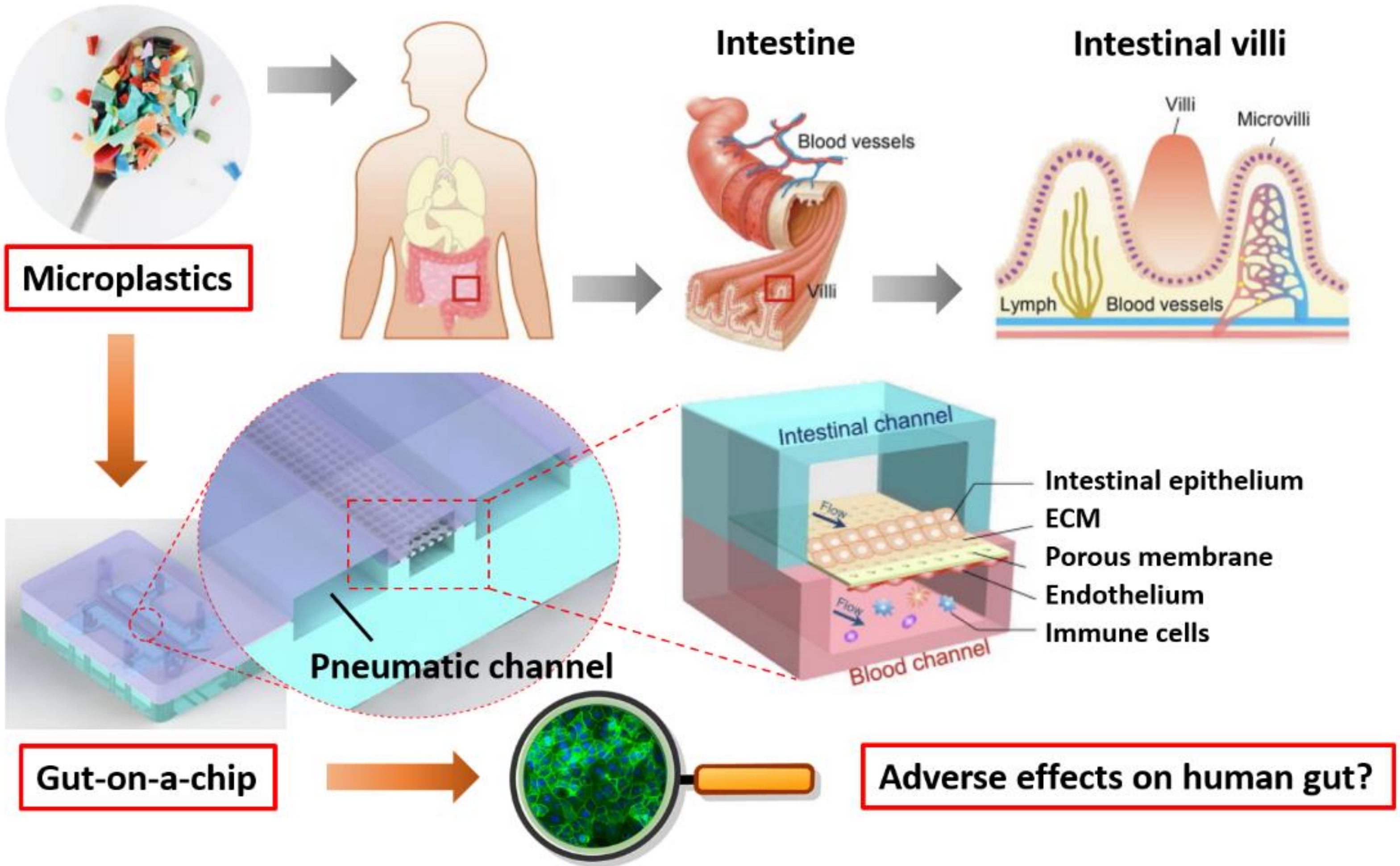

Intestine
Intestinal villi
Blood vessels
Villi
Villi
Microvilli
Lymph
Blood vessels
Microplastics
Intestinal channel
Intestinal epithelium
ECM
Porous membrane
Endothelium
Immune cells
Flow
Flow
Blood channel
Pneumatic channel
Gut-on-a-chip
Adverse effects on human gut?

Detection of enrofloxacin in Foods

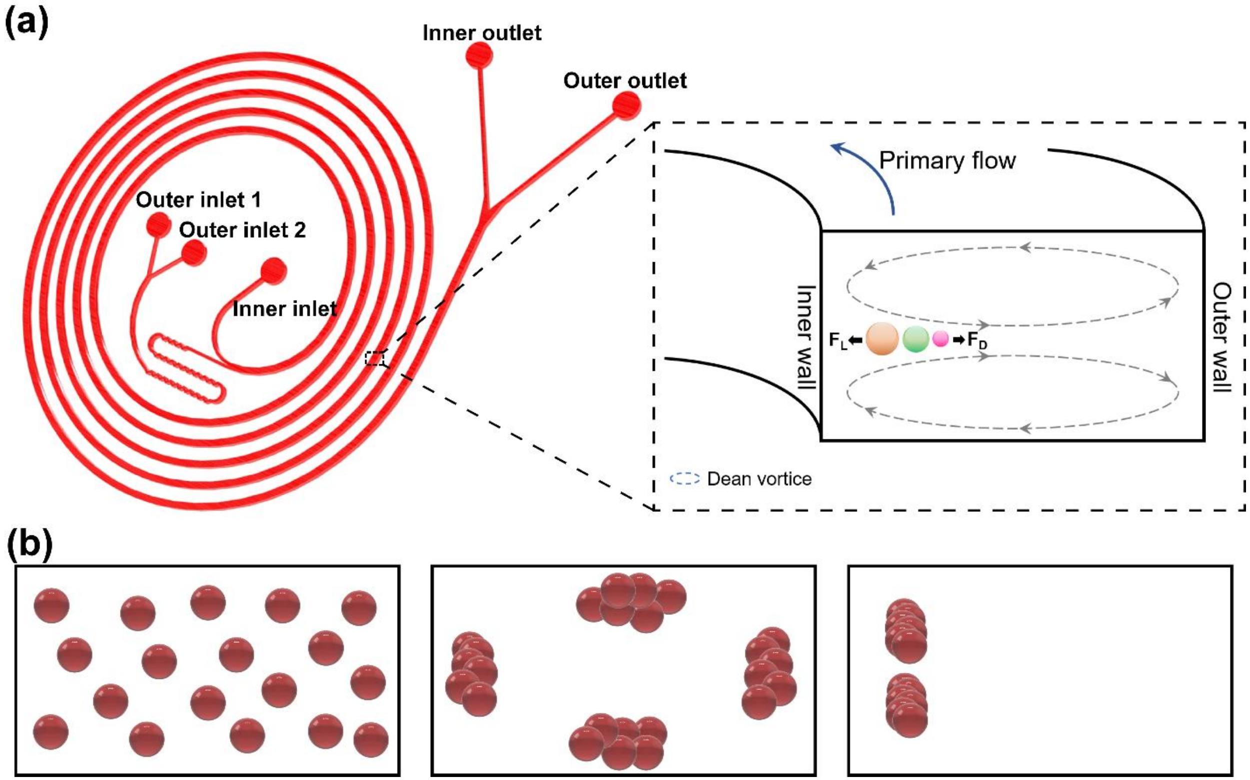

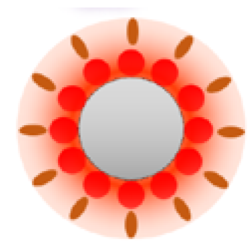

QDs@MIPs

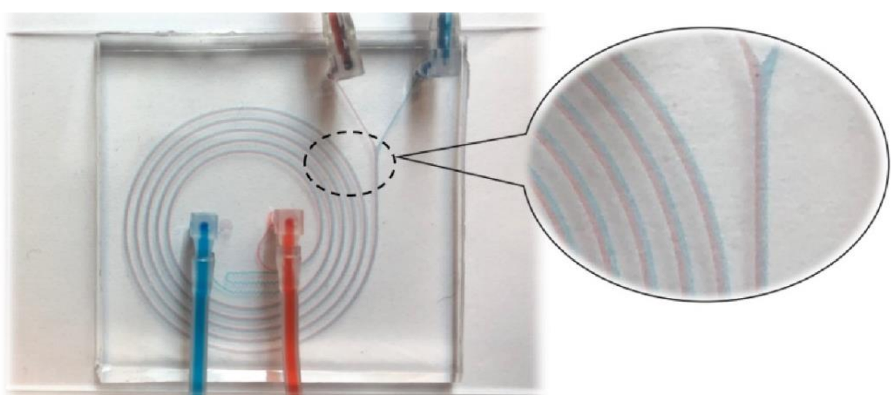

Quantum dots-based molecular imprinting fluorescence sensor

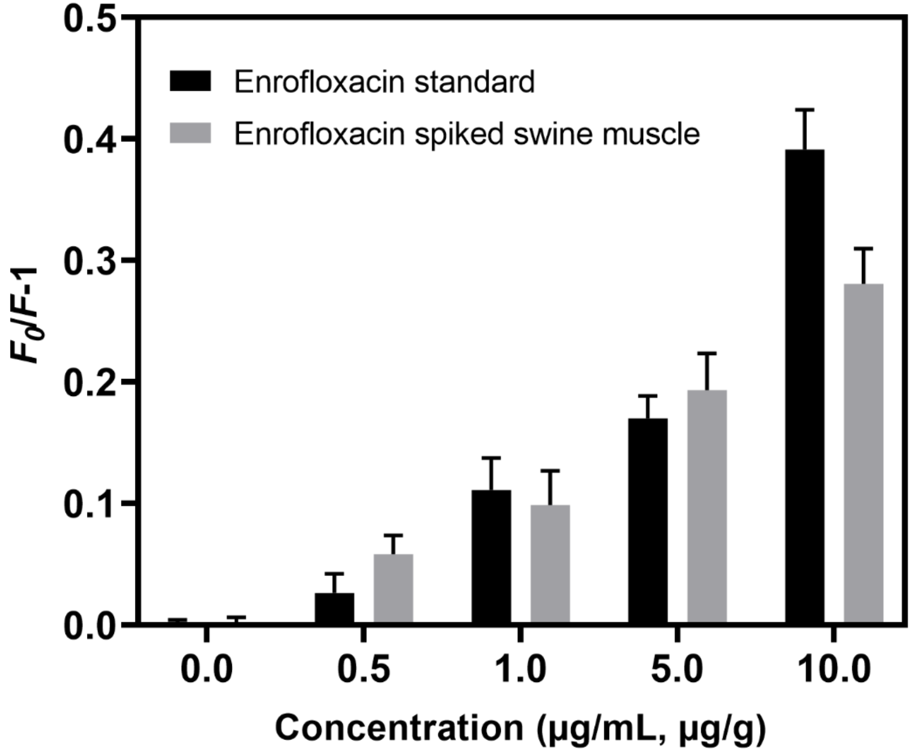

Fluorescence quenching amounts of QDs@MIPs after passing through the spiral microchannel. Enrofloxacin standard solutions or enrofloxacin spiked swine muscle sample extractions were injected for MIPs adsorption and fluorescence quenching. (n=5)

Thank You